Article

Structure and Branching of Unstable Modes in a Swirling Flow

Vadim Akhmetov

Department of Applied Mathematics, Moscow State University of Civil Engineering (National Research University), 129337 Moscow, Russia; AhmetovVK@mgsu.ru

Abstract: Swirling has a significant effect on the main characteristics of flow and can lead to its fundamental restructuring. On the flow axis, a stagnation point with zero velocity is possible, behind which a return flow zone is formed. The apparent instability leads to the formation of secondary vortex motions and can also be the cause of vortex breakdown. In the paper, a swirling flow with a velocity profile of the Batchelor vortex type has been studied on the basis of the linear hydrodynamic stability theory. An effective numerical method for solving the spectral problem has been developed. This method includes the asymptotic solutions at artificial and irregular singular points. The stability of flows was considered for the values of the Reynolds number in the range $10 \leq \mathrm{Re} \leq 5 \times 10^6$. The calculations were carried out for the value of the azimuthal wavenumber parameter $n = -1$. As a result of the analysis of the solutions, the existence of up to eight simultaneously occurring unstable modes has been shown. The paper presents a classification of the detected modes. The critical parameters are calculated for each mode. For fixed values of the Reynolds numbers $60 \leq \mathrm{Re} \leq 5000$, the curves of neutral stability are plotted. Branching points of unstable modes are found. The maximum growth rates for each mode are determined. A new viscous instability mode is found. The performed calculations reveal the instability of the Batchelor vortex at large values of the swirl parameter for long-wave disturbances.

Keywords: swirling flow; hydrodynamic stability; spectral problem; neutral curves; singular points

1. Introduction

Swirling flows of liquid and gas are often found in nature (tornadoes, funnels). They are widely used in various technical applications. Current potential areas of application for swirling flows includes the following [1,2]: the creation of efficient facilities for the combustion of pulverized fuel for modern thermal power plants; optimization of the operation of gas turbine engines through the use of swirling flow in combustion chambers; the development and design of cyclone-type devices for cleaning gas from dust, separating particles, separating liquid mixtures, for example, for cleaning manufactured petroleum, as well as vortex nozzles for liquid spraying; and the usage of the Ranque–Hilsch effect in vortex tubes for the separation of flows by temperature.

In hydraulic engineering, swirling flows are used for the development of suction pipes for hydraulic turbines, vortex spillways, counter-vortex energy absorbers, counter-vortex aerators for the cleaning of natural and artificial reservoirs, settling ponds and storage tanks in the biological and chemical industries.

Studies of the hydrodynamic stability of swirling flows are very important. The loss of flow stability often leads to disruption of the designated mode of operation, through increased vibration effects and, ultimately, damage.

There are several general criteria for evaluating the stability of swirling flows. For a flow of the free vortex type, they were formulated in [3,4]. These criteria are sufficient. However, they do not accurately define the parameters of flow stability.

The main tool for investigating the hydrodynamic stability of vortex flows is numerical simulation based on the perturbation method. In recent years, much attention has been paid to the study of the Batchelor vortex (often called *Q*-vortex) [5]. First, the stability

of Batchelor's trailing vortex model with respect to non-axisymmetric perturbations of the form $\exp[i(\alpha z + n\varphi - \alpha ct)]$ for the inviscid flow was studied numerically by Lessen et al. [6]. The authors paid particular attention to disturbances with $n \leq -1$, since they proved to be more unstable than disturbances with positive n.

The authors went on to numerically investigate the effect of viscosity on the stability of a free vortex [7]. The smallest critical Reynolds number corresponded to disturbances with $n = -1$. Two viscous modes of Q-vortex instability for $n = 0$ and $n = 1$ were found in the works [8,9]. The maximal growth rate of viscous modes decreases monotonically with increasing Reynolds number $\text{Re} \rightarrow \infty$.

In the inviscid formulation, the transition from an absolute instability to a convective one for the Batchelor Q-vortex, was studied by Olendraru et al. [10]. They observed absolute instability modes $n = -1, -2, -3$ in jet flows. For wake-type flows, absolute instability was found only for the $n = -1$ mode. The works [11–13] provide a generalization of these studies with allowance for the compressibility of the flow.

Article [14] presents similar studies for the Rankine vortex in the inviscid formulation, and paper [15] shows it for shear swirling flows.

A selective analysis of the absolute instability for a Q-vortex with allowance for viscosity was conducted by the method of direct numerical simulation in [16]. Systematic and detailed studies in a wide range of Reynolds numbers were performed by Olendraru and Sellier [17]. The investigation of the absolute and convective instability in the compressible boundary layer on a rotating disk are presented by Turkyilmazoglu et al. [18–20].

The results of experiments on the stability of swirling flows and the structure of the axial recirculation zone during vortex breakdown are presented in the works [21–25].

Oberleithner et al. [26] considered the issues of global instability which follow a vortex breakdown. The relation between the vortex breakdown phenomenon and the stability of the swirling flow is shown in [27].

In regard to the problems of heat flow separation in Ranque–Hilsch tubes, flow stability was studied in the work [28] and in article [29] for a stratified medium.

The analysis of scientific works shows great interest in the study of the stability of swirling flows. The Batchelor vortex has a velocity distribution in which such flows are significantly reduced. The matter of Batchelor vortex stability is therefore an important and urgent problem. Currently, the effect of viscosity on stability characteristics has not been studied in sufficient depth. There is no detailed topography of instability in the presence of instability modes occurring simultaneously in the flow. The stability of a Q-vortex for large swirl numbers has not been investigated sufficiently.

The subject of this work is the study of the stability of swirling flow using the Batchelor vortex as an example. For this, an effective numerical method has been developed taking into account the behavior of solutions at singular points. This method is used to solve a multiparameter spectral problem.

The aim of this work is to study the interaction of unstable modes. The novelty of the work consists of a detailed study of the spectrum of instability and calculation of the critical parameters of the swirling flow.

2. Hydrodynamic Flow Model and Numerical Method

Studies of the hydrodynamic stability of swirling flows of a viscous incompressible fluid are based on the Navier–Stokes equations. In a cylindrical coordinate system (r, φ, z), with respect to the velocity-pressure variables, it can be represented as follows that the flow is axisymmetric [30,31]:

$$\frac{\partial V_z}{\partial t} + V_z \frac{\partial V_z}{\partial z} + V_r \frac{\partial V_z}{\partial r} = -\frac{\partial p}{\partial z} + \frac{1}{\text{Re}} \left(\frac{\partial^2 V_z}{\partial r^2} + \frac{1}{r} \frac{\partial V_z}{\partial r} + \frac{\partial^2 V_z}{\partial z^2} \right) \tag{1}$$

$$\frac{\partial V_\varphi}{\partial t} + V_z \frac{\partial V_\varphi}{\partial z} + V_r \frac{\partial V_\varphi}{\partial r} + \frac{V_r V_\varphi}{r} = \frac{1}{\text{Re}} \left(\frac{\partial^2 V_\varphi}{\partial r^2} + \frac{1}{r} \frac{\partial V_\varphi}{\partial r} + \frac{\partial^2 V_\varphi}{\partial z^2} - \frac{V_\varphi}{r^2} \right) \tag{2}$$

$$\frac{\partial V_r}{\partial t} + V_z \frac{\partial V_r}{\partial z} + V_r \frac{\partial V_r}{\partial r} - \frac{V_\varphi^2}{r} = -\frac{\partial p}{\partial r} + \frac{1}{\mathrm{Re}} \left(\frac{\partial^2 V_r}{\partial r^2} + \frac{1}{r}\frac{\partial V_r}{\partial r} + \frac{\partial^2 V_r}{\partial z^2} - \frac{V_r}{r^2} \right) \tag{3}$$

$$\frac{1}{r}\frac{\partial(V_r\,r)}{\partial r} + \frac{\partial V_z}{\partial z} = 0 \tag{4}$$

Here, V_z, V_r, V_φ are axial, radial and azimuthal velocity components, respectively, p is pressure, and Re is the Reynolds number.

The profiles of the axial V_z and azimuthal V_r components of the velocity of free swirling flows and internal flows in channels (with the exception of the near-wall region) can be rather well described through the following expressions [32,33]:

$$V_z = W_1 + W_2 \exp(-br^2), \quad V_\varphi = \frac{K}{r}[1 - W_2 \exp(-br^2)], \tag{5}$$

where W_1, W_2, K and b are constants defined empirically, and r is the dimensionless distance from the axis. Using elementary transformations, the profiles (5) can be reduced to the following form:

$$U = \exp(-r^2), \quad W = \frac{q}{r}(1 - \exp(-r^2)) \tag{6}$$

where q is the swirl number (the inverse value to the Rossby number). Profiles (6) are deduced from Batchelor's self-similar solution of the Navier–Stokes equations for a viscous swirling wake under the assumption that the flow is plane-parallel [5]. Distribution (6) for $q = 1$ is shown in Figure 1.
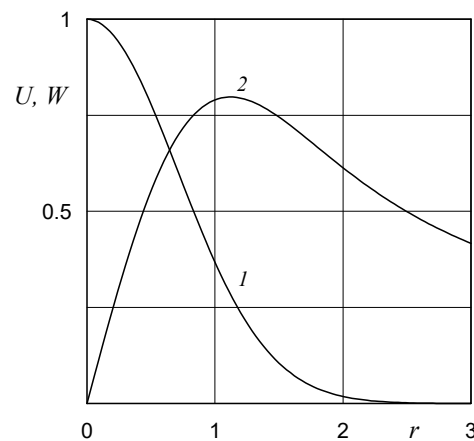

Figure 1. Batchelor's profiles of axial U and azimuthal W velocities (curves 1, 2).

Let us consider small flow disturbances (7) as solutions of the linearized Navier–Stokes equations of the periodic traveling wave type (normal modes):

$$\{V_z', V_r', V_\varphi', p'\} = \{F, iS, H, P\} \exp[i(\alpha z + n\varphi - \alpha ct)] \tag{7}$$

in which α is the wave number; n is the disturbance mode $(n = 0; \pm 1; \pm 2; \ldots)$ and where positive values of n correspond to the propagation of the wave in the direction of swirl and negative ones in the opposite direction; c is the wave propagation speed; i is the imaginary unit; and $F(r), S(r), H(r)$ and $P(r)$ are the complex amplitude functions.

After the linearization of Equations (1)–(4) and the substitution of expressions (6) and (7) for complex-valued amplitude functions, we obtain the following system of equations [7]:

$$r^2 \gamma F + \alpha r^2 P + r^2 SU' = \frac{1}{i\mathrm{Re}}[r\,(r\,F')' - (\alpha^2 r^2 + n^2)F] \tag{8}$$

$$r^2 \gamma S + 2rHW - r^2 P' = \frac{1}{i\mathrm{Re}}[r(rS')' - (\alpha^2 r^2 + n^2 + 1)S - 2nH] \tag{9}$$

$$r^2\gamma H + r^2 S\left(W' + \frac{W}{r}\right) + rnP = \frac{1}{i\mathrm{Re}}[r(rH') - (\alpha^2 r^2 + n^2 + 1)H - 2nS] \tag{10}$$

$$\alpha rF + (rS)' + nH = 0 \tag{11}$$

where $\gamma = \alpha(U - c) + nW/r$, prime designates the derivative with respect to r.

The boundary conditions for Equations (8)–(11) are derived by Batchelor & Gill [34]: The set of conditions is presented in Table 1.

Table 1. The boundary conditions.

n	Amplitude Functions
	$r = 0$
$n = 0$	$S = H = 0$, F, P are bounded
$n = \pm 1$	$F = P = 0$
$\lvert n \rvert > 1$	$S = H = F = P = 0$
	$r = \infty$
$\forall n$	$S = H = F = P = 0$

It is possible to consider the disturbances (8) as periodic in respect of z, the amplitude of which changes with time. Then, α is a real number ($\alpha = 2\pi/\lambda$, where λ is the disturbance wave length), and $c = c_r + ic_i$ is an imaginary one; c_r is the speed of propagation of the disturbance in the direction z (phase velocity), c_i is the rate of increase of the disturbance in time. The amplitudes of disturbance (8) decay for $c_i < 0$ (the flow is stable), and they increase over time (the flow is unstable) for $c_i > 0$. Thus, c_i must be defined as a function of α.

In another case, we investigate the behavior of periodic perturbations (8) with an amplitude that changes in the z direction; however, this does not depend on time. It follows that the oscillation frequency $\omega = \alpha_r c$ should be considered as real (c is the phase velocity) and the value $\alpha = \alpha_r + i\alpha_i$ as complex; α_i determines the spatial growth rate of the perturbation. The disturbance dies out (the flow is stable) for $\alpha_i > 0$, and it grows for $\alpha_i < 0$ (the flow is unstable). In this case, it is important to determine the relation between α_i and ω.

The method for eigenvalues calculation includes several stages. First, we obtain asymptotic solutions near the singular points $r = 0$ and $r = \infty$ using the Frobenius method. This method for solving the stability problem was first introduced by Lessen & Paillet [9]. The same approach is used in this work. We transfer the boundary conditions from the points $r = 0$ and $r = \infty$ and to the points $r = r_a$ and $r = r_d$, respectively. The solution at these points is defined as a power series. A detailed description of the applied method is presented in [35]. Then, we perform numerical integration from r_a and r_d inside the computational domain to the point r_c ($r_a < r_c < r_d$), at which the solutions are merged in accordance with the condition

$$\sum_{j=1}^{3} a_j y_{i,j} = \sum_{j=1}^{3} a_{j+3} y_{i,j+3} \quad (i = 1, 2, \ldots, 6) \tag{12}$$

where $y_{i,j}$ are solutions obtained by integration from r_d to r_c, $y_{i,j+3}$ are solutions obtained by integration from r_a to r_c and a_j is an arbitrary constant. The vanishing of the determinant for the linear system (12) is achieved by selecting c_r, c_i (or α_r, α_i) according to Newton's method. To calculate the eigenvalues, the parameter step was determined automatically by the number of iterations k_{it} in Newton's method for solving the characteristic equation. The value k_{it} was in the interval $3 \leq k_{it} \leq 7$. In order to accelerate convergence, the next initial value of the eigenvalue was determined by linear extrapolation using Newton's method.

We write the system of Equations (8)–(11) in the form of six differential equations of the first order $z' = f(r, z)$ for numerical integration. The solution of this system was

determined on the basis of the Kutta–Merson method with an automatic selection of the integration step.

When solving problems of hydrodynamic stability, the fundamental difficulty in the implementation of this method is the rapid (parasitic) growth of one or several solutions during integration. As a result of this growth the linear independence of solutions is lost. In order to avoid this, we applied an orthogonalization procedure for each calculated point.

The values $r_a = 0.01$ and $r_c = 2$ were used in the calculations; the r_d value was selected for each set of parameters individually, based on the specified accuracy of determining the eigenvalue and varied from $r_d = 2.7$ to $r_d = 150$. The widest region of integration was required for long-wavelength perturbations at large values of the Reynolds numbers and the swirl parameter.

3. Results and Discussion

Let us consider the boundary value problem (8)–(11), in which there are three defining parameters: Re, q and α. We investigate the stability of the flow (6) for the wavenumber value $n = -1$, since, according to [7,8], this type of disturbance is the most dangerous. The eigenvalue $c = c_r + ic_i$ of the considered spectral problem for $c_i > 0$ determines the mode of temporal instability. This study shows the existence of several unstable modes that can be simultaneously observed in the flow. Each numbered mode is characterized by a set of parameters that determine the critical values of the Reynolds number Re_c^m, swirl q_c^m, and wavenumber α_c^m at which instability appears. This set corresponds to an eigenvalue c_{rm}, $c_{im} \approx 0$, from which it is possible to construct numerically a parametric continuation with respect to Re, q, or α. The most important is the continuation by the use of the Reynolds number. Table 2 shows the calculated values of Re_c^m, α_c^m and q_c^m at critical points for eight detected instability modes.

Table 2. Critical values of unstable modes.

Mode	Re_c^m	α_c^m	q_c^m
1	13.905	0.415	0.337
2	43.934	0.5012	0.6603
3	165.56	0.5962	0.4576
4	428.086	0.5062	0.6095
5	887.79	0.5547	0.6403
7	1579.73	0.6054	0.700
8	3526.77	0.5679	0.6131

First, mode 1 was discovered by Lessen and Paillet [7]. It has the smallest critical Reynolds number, the largest growth rate and causes the development of convective instability in the flow. In addition, this is the only mode that is unstable in both non-swirling and swirling flows. The critical parameters presented for it in Table 1 completely correspond to the previously obtained values in the papers [7,9].

The modes investigated are of a different nature. Modes 1 and 3–8 are inviscid. The maximal growth rate in this case tends to a certain limiting positive value $\omega_i = \alpha c_i \to \text{const} \neq 0$ at Re $\to \infty$. Table 3 presents the maximal growth rate ω_i^* for inviscid modes 1 and 3–6, the critical values of the wavenumber α_* and swirl q_* which correspond to them and were calculated for Re $= 10^5$. The obtained eigenvalues can be considered as asymptotic for Re $\to \infty$, since they change insignificantly with the increases in Re. Comparison with the corresponding values of the inviscid theory [9] confirms the reliability and high accuracy of the results obtained in the work.

Table 3. Comparison with the results of the inviscid theory.

Mode	Re = 10^5			Re = ∞ (Reference [9])		
	q_*	α_*	ω_i^*	q_*	α_*	ω_i^*
1	0.4581	0.8117	0.2424	0.46	0.81	0.2424
3	0.7534	0.5518	0.1112	0.75	0.55	0.1116
4	0.7972	0.5402	0.0797	0.8	0.54	0.08046
5	0.8091	0.5263	0.0609	0.82	0.53	0.06222
6	0.8098	0.5146	0.0483	0.83	0.53	0.05030

Comparison of the critical Reynolds number values for inviscid modes 1 and 3–8 (Table 2) and the corresponding values of the maximal growth rate (Table 3) shows that the smallest critical Reynolds number corresponds to the more unstable mode.

Mode 2 is viscous. For it, $\omega_i \to 0$ when Re $\to \infty$. It was first discovered in the work [36] and studied in more detail in [37]. Two other viscous unstable modes for flow (7) were found in [8,9]. One of them was observed for axisymmetric disturbances ($n = 0$), the other (more unstable) for non-axisymmetric disturbances with a positive azimuthal wavenumber ($n = 1$).

Figure 2 shows the spectral characteristics for mode 2. The phase velocities of disturbances with wavenumbers corresponding to the maximal growth rate are negative, i.e., unstable disturbances in this case propagate upstream. Table 4 presents comparison of the spectral characteristics for mode 2 with the results of [17]. The viscous mode 2 has growth rates that are higher by an order of magnitude than the previously obtained mode at $n = 1$.
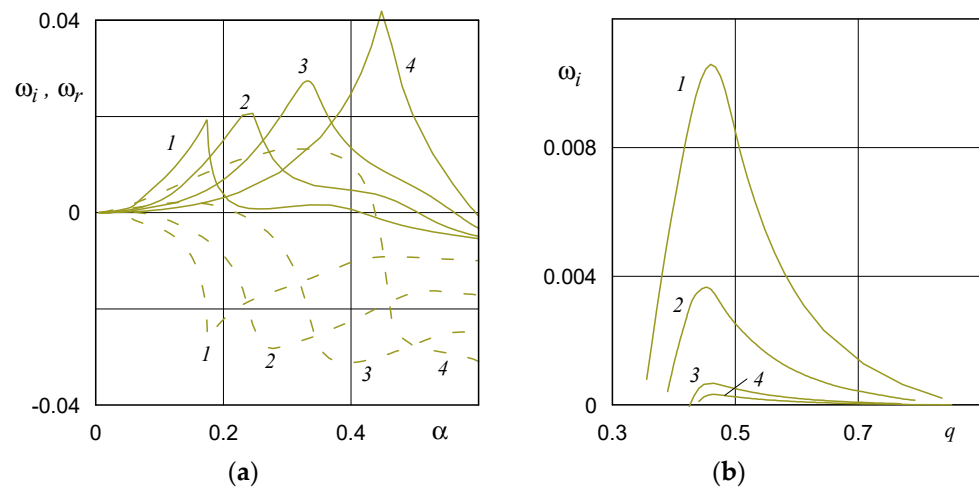

Figure 2. (**a**) The growth rate (solid lines) and oscillation frequency (dashed lines) vs. the wavenumber for Re = 100, q = 0.3; 0.4; 0.5; 0.6 (curves 1–4); the growth rate has a peak-like distribution. (**b**) Dependence of the growth rate from the swirl for α = 0.3, Re = 300, 1000, 5000, 10,000 (curves 1–4).

Table 4. Comparison of viscous modes.

	$n = -1$ (Mode 2)			$n = 1$ (Reference [17])	
Re	100	1000	5000	100	1000
$\omega_i^* \times 10^2$	8.8	2.83	1.28	0.96	0.166
q_*	0.7	0.7	0.7	0.475	0.24
α_*	0.824	0.868	0.848	0.418	0.21

Let us turn to the study of eigenvalue solutions for the problem under consideration in the plane of free parameters (α, q) for Re = const. In this regard, we note one important property of eigenvalue solutions. There are points in the space Re, q and α at which the

eigenvalue problem has a multiple root $c^{(k)} = c^{(m)}$. This means that the solutions for the two modes coincide at such a point, and the branching of these modes occurs in close vicinity. In this case, different pairs (k, m) from the set of unstable modes existing at the selected value Re can branch.

The regions of stability and instability of the flow (6) to disturbances (7) are separated in the plane (α, q) of the neutral curve by the line on which the condition $\omega_i = 0$ is satisfied. A corresponding neutral curve can be plotted for each mode of instability. The neutral curve of mode m is described by a separate closed contour only for values Re $>$ Re$_c^m$, which are close to the critical one for this mode, for example, modes 1 and 2 for Re = 60 (Figure 3), mode 4 for Re = 450 (Figure 4c) and mode 5 for Re = 1000 (Figure 4d). When we move along Re from the critical point, its bifurcations appear with newly emerging modes. In this case, the shape of the instability region changes qualitatively. An abrupt change in the boundaries of the instability regions occurs, and the neutral curves are combined into a single curve of complex shape with points of self-intersection.

Let us consider the branching process in more detail using the first two modes as an example. When the Reynolds number increases, the regions of instability of the two modes intersect, and the neutral curves are combined into one curve. Part of this curve corresponds to the first mode, while the other corresponds to the second. Figure 4a shows the typical instability region for Re = 140 with branch point $q_b = 0.689$. Inside this region, the flow instability (8) can be determined by either one or two modes simultaneously, depending on the values (α, q).

When the parameter q passes through q_b, two branching modes exchange parts of the dependences $\omega_r(\alpha)$, $\omega_i(\alpha)$ and, as a consequence, by the values $\alpha_{\max}$, $\alpha_{\min}$ characterizing the boundaries of the regions of instability. This mode transformation is clearly seen from Figure 5 plotted for modes 1 and 2. The values of the α wavenumber, at which $\omega_i = 0$ in the upper part of the neutral curve, are 1.323 for modes 1 and 2; 0.67 for $q = 0.68$ (Figure 5a) and 0.653; and 1.305 for $q = 0.69$ (Figure 5b). At the branch point $q_b = 0.689$ (the branch points are indicated by the dotted line in Figure 4), the original eigenvalue problem has a multiple root, and the phase velocities and growth rates of the two modes coincide: $\omega_r^1 = \omega_r^2 \approx 0.027$, $\omega_i^1 = \omega_i^2 \approx 0.055$ for $\alpha \approx 0.602$.
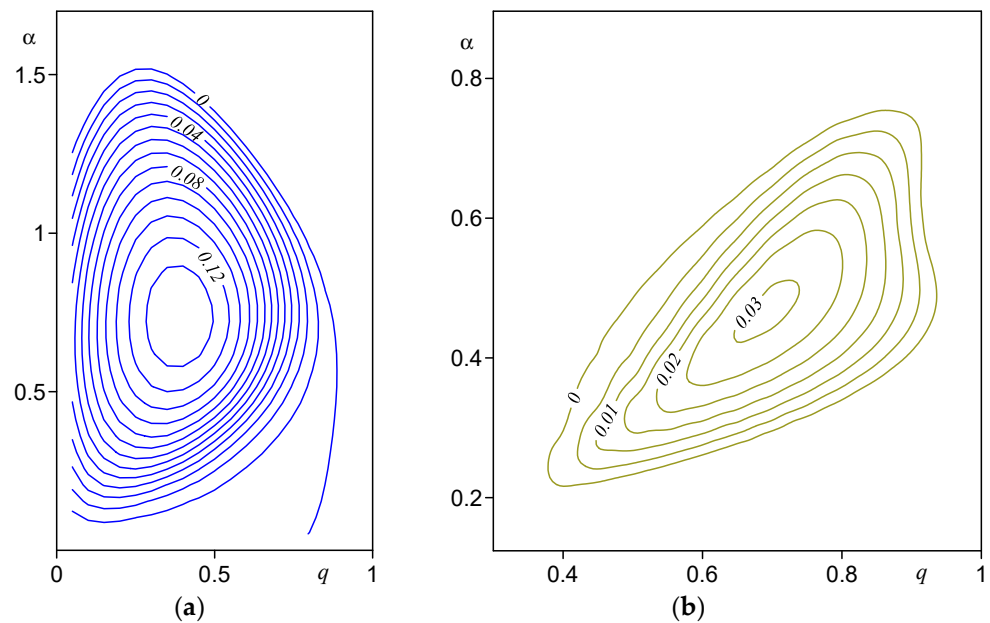

Figure 3. The lines depict the constant growth rate of the values $\omega_i = \alpha c_i = $ const in plane (α, q) at Re = 60: (**a**) mode 1; (**b**) mode 2. The outer contour corresponds to the neutral curve on which $\omega_i = 0$. The flows are unstable inside it, and one is stable outside it.
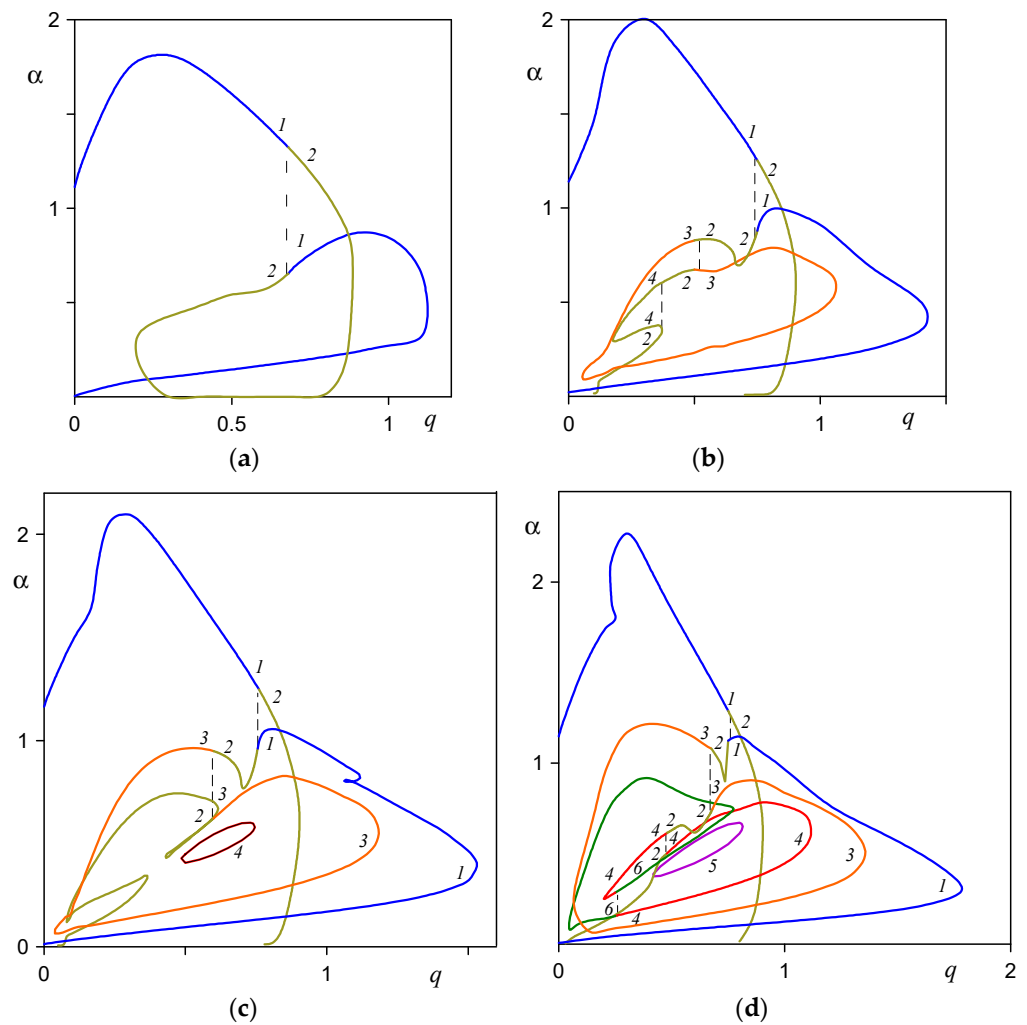
Figure 4. Neutral curves: Re = 140; 300; 450; 1000 (**a**–**d**); modes 1–6. The dashed lines correspond to the q values at the branch points.
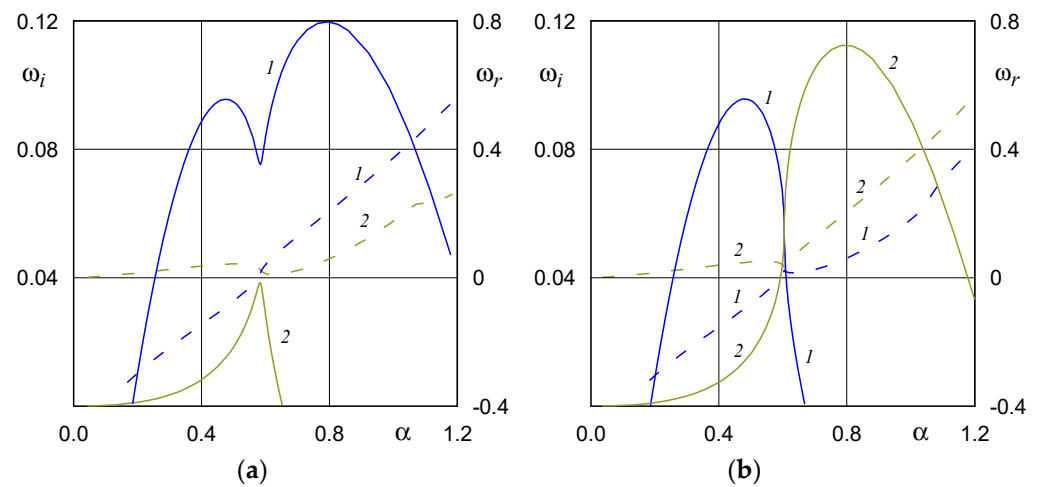

Figure 5. The growth rate ω_i (solid lines) and oscillation frequency ω_r (dashed lines) vs. the wavenumber for modes 1 and 2 (curves 1–2) at Re = 140: (**a**) $q = 0.68$; (**b**) $q = 0.69$. In the particular case, when Re = 115 at the branch point $q = 0.65$ of modes 1 and 2, perturbations (8) generate standing waves: $\omega_r^1 = \omega_r^2 = 0$, $\omega_i^1 = \omega_i^2 = 0.061$ for $\alpha = 0.527$.

Mode branching occurs in a similar way in all other cases, and new branch points appear with increasing Re with new unstable eigen solutions of the spectral problem under consideration.

Figure 4d shows the neutral curves for six unstable modes for Re = 1000. The instability region of mode 5 has a separate contour. Neutral curves for other modes are depicted as one curve with branch points q_b = 0.225, 0.495, 0.675 and 0.76 between modes 4 and 6, 2 and 4, 2 and 3 and 1 and 2 respectively. Parts of the curve can be seen to correspond to modes 1, 2, 4, 6, 4, 2, 3, 2, 1 if one moves around it in the positive direction from the point $q = 0$, $\alpha = 1.15$. Note that mode 6 is formed from a part of mode 2 for $900 < \text{Re} < 1000$, and its neutral curve does not have a separate closed contour. This is distinct from all other investigated modes.

The neutral curves have the most composite structure, including eight branch points at Re = 5000 (Figure 6). The neutral curves of the first five modes are depicted by one intersecting curve with branch points q_b = 0.37, 0.73, 0.745, 0.54 and 0.68 between modes 1 and 3, 3 and 1, 1 and 2, 2 and 5 and 2 and 4 respectively. When passing along it in the positive direction from the point $q = 0$, $\alpha = 1.18$, the sections of the curve correspond to modes 1, 3, 1, 3, 1, 2, 5, 2, 4, 2, 3, 1. Neutral curves of modes 6–8 are depicted by two closed curves. The first one contains modes 6 and 7, the second modes 6, 7 and 8 with branch points q_b = 0.36, 0.43, 0.71 and 0.78 between modes 8 and 7, 6 and 7, 7 and 6 and 7 and 8. Table 5 presents the set of branch points of modes 1–8 for all the calculations performed.
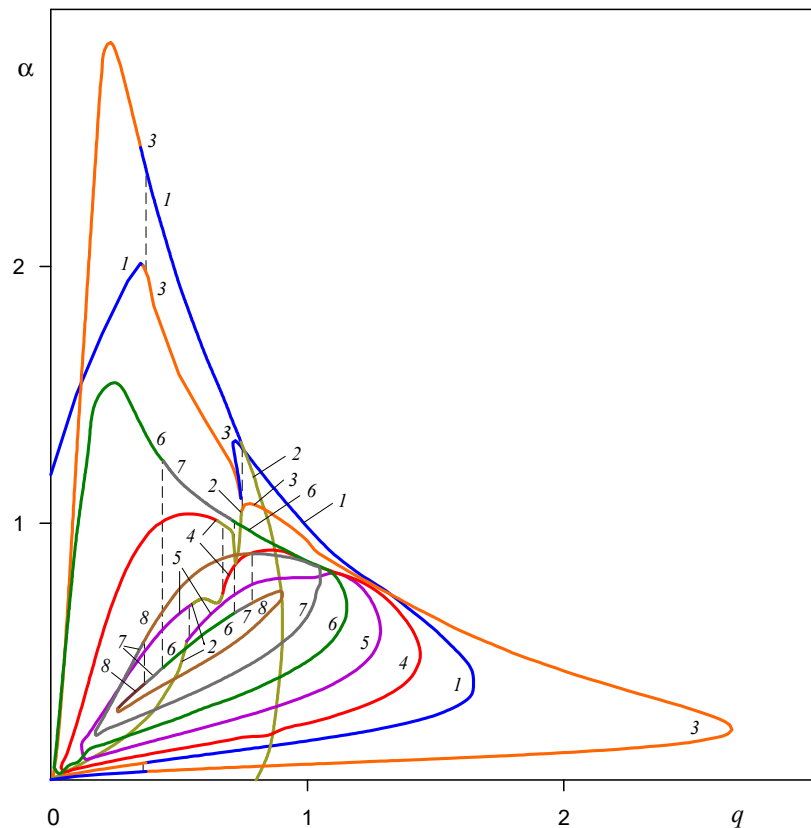

Figure 6. Neutral curves for Re = 5000; modes 1–8 (curves 1–8). The dashed lines correspond to the q values at the branch points. Mode 3 is unstable at a much larger swirl of the flow compared to the known value $q = 1.5$ for mode 1.

Table 5. Branching points of modes.

Re	$q_b(k,m)$				
140	0.689 (1,2)	-	-	-	-
300	0.74 (1,2)	0.52 (3,2)	-	-	-
450	0.755 (1,2)	0.595 (2,3)	-	-	-
1000	0.76 (1,2)	0.675 (2,3)	0.495 (2,4)	0.225 (4,6)	-
5000	0.78 (7,8)	0.745 (1,2)	0.73 (3,1)	0.71 (7,6)	-
	0.68 (2,4)	0.54 (2,5)	0.43 (6,7)	0.37 (1,3)	0.36 (8,7)

The present calculations have established that modes 4–6 are also unstable at $q > 1.5$. Figure 7 shows the dependences q_{max} on the Reynolds number for modes 1 to 7. The behavior of modes 4–6 (curves 4–6) with increasing Re is the same as for the previously studied mode 3 (curve 3), and the highest swirl values are $q = 3.06, 1.654$ and 1.575 for $Re = 8 \times 10^5, 5 \times 10^5$ and 1×10^5 and $\alpha = 0.3, 0.6$ and 0.6 for modes 4–6, respectively. The dependences for inviscid modes 7 and 8 have a similar characteristic of change, however, these modes remain stable at $q > 1.5$. The maximum calculated values, at which modes 7 and 8 are unstable, are $q = 1.409$ and 1.366 for $Re = 5 \times 10^5$ and $\alpha = 0.7$.
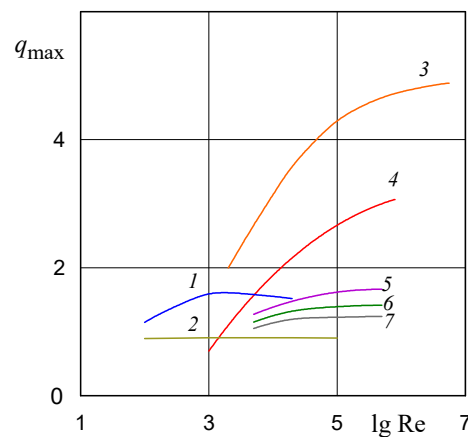

Figure 7. The maximum values of the swirl q, at which the flow is unstable: modes 1–7 at $\alpha = 0.4$; 0.6; 0.2; 0.3; 0.6; 0.7; 0.8 (curves 1–7). The swirl value, at which the instability is observed for mode 3, reaches $q = 4.882$ at $Re = 5.5 \times 10^6$.

For moderate Reynolds numbers $Re < 2000$, the value of the maximum swirl, at which mode 1 (curve 1) is unstable, increases. It subsequently decreases with increases in Re. For $Re = 10^5$, mode 1 becomes stable for $q > 1.5$, corresponding to the results previously obtained using the inviscid theory [7]. For the sole viscous mode 2, the maximum swirl value, at which the flow instability remains, practically unchanged with increasing Re, is $q = 0.9$ for $\alpha = 0.6$.

Now, let us consider perturbations (7), which are periodic in time. In this case, the oscillation frequency $\omega = \alpha_r c$ should be considered as real, and the wave number α as complex. When $\alpha_i > 0$ the disturbances dampen and when $\alpha_i < 0$, they grow. Negative values correspond to the propagation of disturbances upstream.

Analysis of the spatial flow instability (6) shows that the detected modes remain unstable in space. Thus, all of the basic conclusions obtained in the study of temporal instability are preserved: The most unstable mode is inviscid mode 1, there is the only one viscous mode 2, neutral curves also contain branch points, and flow instability persists at large values of the swirl parameter q. For example, the maximum growth rates $-\alpha_i^*$ for mode 3 are 0.00608, 0.01298 and 0.01581 for $q = 2.4$; at the same time, $\omega = -2.077, -2.091$ and -2.102 for $Re = 5 \times 10^3, 10^4$ and 2×10^4, respectively.

Figure 8 shows a typical picture of the growth rate change due to the oscillation frequency for the first four modes. For a given oscillation frequency at Re ≈ 3450, the source eigenvalue problem has a multiple root, and the values of α_i, α_r for modes 2 and 3 coincide. When the Reynolds number increases, an explosive change appears in the boundaries of the instability region for each of these modes. For example, the values ω on the upper part of the neutral curve ($\alpha_i = 0$) in the (ω, Re) plane are $\omega = 0.451$, 0.454 and 0.133 at $q = 0.7$ for mode 2. The analogous values for mode 3 are $\omega = 0.119$, 0.126 and 0.457 for Re = 3300, 3400 and 3500, respectively. The branching of modes 1 and 2 and 2 and 4 occurs in the same way for Re ≈ 7000 and ω ≈ 0.06.
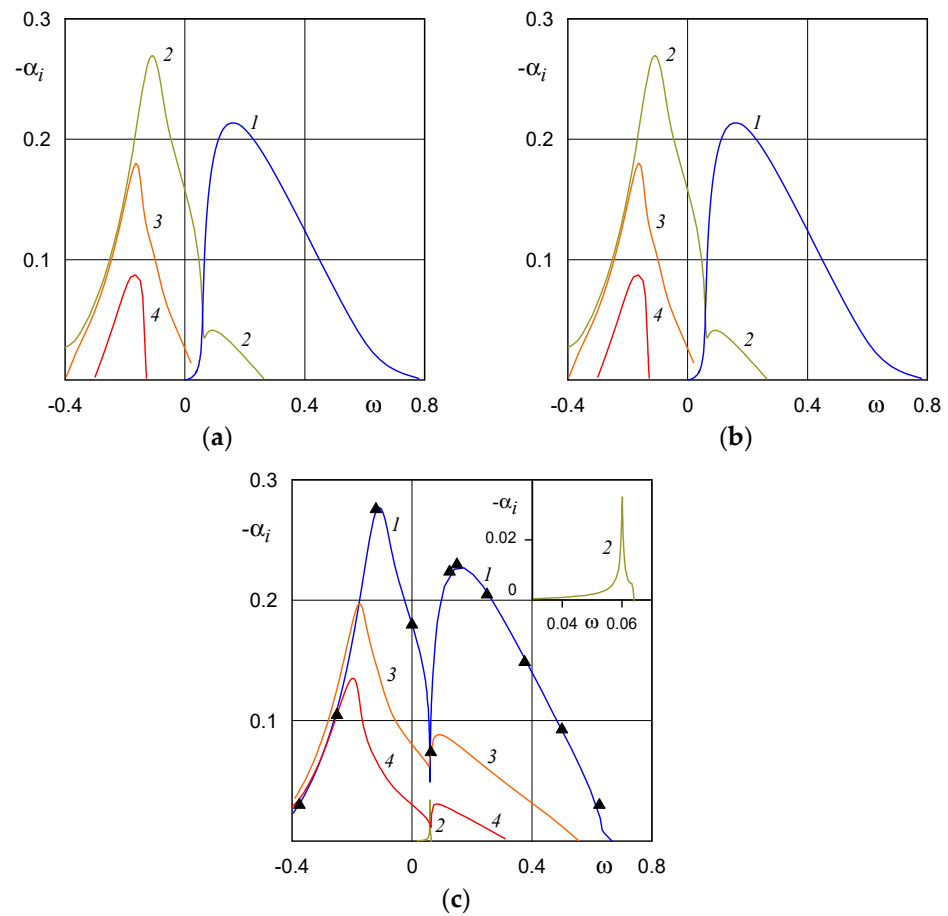

Figure 8. The growth rate from the oscillation frequency (spatial instability) for modes 1–4 (curves 1–4) for $q = 0.7$ (**a**) Re = 1000; (**b**) Re = 5000; (**c**) Re = 10,000. The triangular symbols correspond to the inviscid theory. The presence of two local maxima in the depicted relations for modes 1, 3 and 4 is associated with the branch point for ω ≈ 0.06.

For Re = 10^4, mode 1 is the most unstable. The non-viscous modes 3 and 4 are weaker. The growth rate of the viscous mode has a peak-like distribution. The triangular symbols in Figure 8c show the dependence of the growth rate on the frequency for mode 1 obtained on the basis of the inviscid theory [10]. Here, numerical studies were limited by the existence of only one unstable mode. Comparison of the results obtained confirms the reliability of the calculations and explains the nature of growth rates distribution in inviscid modes with two local maxima.

4. Conclusions

The stability problem of a swirling flow in the form of Batchelor's trailing line vortex with respect to non-axisymmetric disturbances has been considered. An efficient numerical

method for studying the spectrum of eigenvalues has been presented. The calculation results show the existence of up to eight simultaneously observed unstable modes.

The behavior of each mode separately and the properties of the full spectrum of modes have been studied. The branching property of eigen solutions has been found and investigated. The coordinates of the branch points have been calculated. This has permitted construction of the curves of neutral stability at fixed values of the Reynolds numbers. It has been shown that the branching of modes and the explosive change in the boundaries of the regions of instability are associated with the existence of multiple roots in the source eigenvalue problem.

The existence of a new viscous mode of instability has been shown. The growth rates of this mode are an order of magnitude higher than the values of other previously known viscous modes. This fact confirms the significant effect of viscosity on the stability of swirling flows.

The phenomenon of vortex breakdown is associated with flow instability. The main contribution to the destabilization of the flow is made by the first fundamental mode of instability. Weaker modes can lead to secondary instability. Studies have shown that in a highly swirling Batchelor vortex flow, it is these modes which remain unstable for long-wave disturbances.

Institutional Review Board Statement: Not applicable.

Informed Consent Statement: Not applicable.

Data Availability Statement: Not applicable.

Conflicts of Interest: The author declares no conflict of interest.

Nomenclature

r, φ, z	radial, azimuthal and axial coordinates, respectively
p	pressure
V	velocity
t	time
Re	Reynolds number
U, W	Batchelor's components of axial and azimuthal velocities, respectively
q	swirl number
F, S, H, P	complex amplitude functions
α	complex axial wave number
n	azimuthal wave number
c	complex eigenvalue
ω	complex frequency
λ	disturbance wavelength

References

1. Gupta, A.K.; Lilley, D.G.; Syred, N. *Swirl Flows*; Abacus Press: Tunbridge Wells, UK, 1984. [CrossRef]
2. Lucca-Negro, O.; O'Doherty, T. Vortex breakdown: A review. *Prog. Energy Combust. Sci.* **2001**, *27*, 431–481. [CrossRef]
3. Leibovich, S.; Stewartson, K.A. Sufficient condition for the instability of columnar vortices. *J. Fluid Mech.* **1983**, *126*, 335–356. [CrossRef]
4. Stewartson, K.; Brown, S.N. Near–neutral center–modes as inviscid perturbations to a trailing line vortex. *J. Fluid Mech.* **1985**, *156*, 387–399. [CrossRef]
5. Batchelor, G.K. Axial flow in trailing line vortices. *J. Fluid Mech.* **1964**, *20*, 645–658. [CrossRef]
6. Lessen, M.; Singh, P.J.; Paillet, F. The stability of a trailing line vortex. Part 1. Inviscid theory. *J. Fluid Mech.* **1974**, *63*, 753–763. [CrossRef]
7. Lessen, M.; Paillet, F. The stability of a trailing line vortex. Part 2. Viscous theory. *J. Fluid Mech.* **1974**, *65*, 769–779. [CrossRef]
8. Khorrami, M.R. On the viscous modes of instability of a trailing line vortex. *J. Fluid Mech.* **1991**, *225*, 197–212. [CrossRef]

9. Mayer, E.W.; Powell, K.G. Viscous and inviscid instabilities of a trailing vortex. *J. Fluid Mech.* **1992**, *245*, 91–114. [CrossRef]
10. Olendraru, C.; Sellier, A.; Rossi, M.; Huerre, P. Inviscid instability of the Batchelor vortex: Absolute-convective transition and spatial branches. *Phys. Fluids* **1999**, *11*, 1805–1820. [CrossRef]
11. Zhou, Z.W.; Lin, S.P. Absolute and convective instability of a compressible jet. *Phys. Fluids A Fluid* **1992**, *4*, 277–282. [CrossRef]
12. Yin, X.-Y.; Sun, D.-J.; Wei, M.-J.; Wu, J.-Z. Absolute and convective instability character of slender viscous vortices. *Phys. Fluids* **2000**, *12*, 1062–1072. [CrossRef]
13. Yadav, N.K.; Samanta, A. The stability of compressible swirling pipe flows with density stratification. *J. Fluid Mech.* **2017**, *823*, 689–715. [CrossRef]
14. Loiseleux, T.; Chomaz, J.M.; Huerre, P. The effect of swirl on jets and wakes: Linear instability of the Rankine vortex with axial flow. *Phys. Fluids* **1998**, *10*, 1120–1134. [CrossRef]
15. Loiseleux, T.; Delbende, I.; Huerre, P. Absolute and convective instabilities of a swirling jet/wake shear layer. *Phys. Fluids* **2000**, *12*, 375–380. [CrossRef]
16. Delbende, I.; Chomas, J.-M.; Huerre, P. Absolute/convective instabilities in the Batchelor vortex: A numerical study of the linear impulse response. *J. Fluid Mech.* **1998**, *355*, 229–254. [CrossRef]
17. Olendraru, C.; Sellier, A. Viscous effects in the absolute-convective instability of Batchelor vortex. *J. Fluid Mech.* **2002**, *459*, 371–396. [CrossRef]
18. Turkyilmazoglu, M. Flow and heat due to a surface formed by a vortical source. *Eur. J. Mech.-B/Fluids* **2018**, *68*, 76–84. [CrossRef]
19. Turkyilmazoglu, M.; Uygun, N. Compressible modes of the rotating-disk boundary-layer flow leading to absolute instability. *Stud. Appl. Math.* **2005**, *115*, 1–20. [CrossRef]
20. Turkyilmazoglu, M.; Cole, J.W.; Gajjar, J.S.B. Absolute and convective instabilities in the compressible boundary layer on a rotating disk. *Theor. Comput. Fluid Dyn.* **2000**, *14*, 21–37. [CrossRef]
21. Blanco-Rodríguez, F.J.; Rodríguez-García, J.O.; Parras, L.; del Pino, C. Optimal response of Batchelor vortex. *Phys. Fluids* **2017**, *29*, 064108. [CrossRef]
22. Delbende, I.; Rossi, M. Nonlinear evolution of a swirling jet instability. *Phys. Fluids* **2005**, *17*, 044103. [CrossRef]
23. Akhmetov, V.K. Stability of counter vortex flows in hydraulic engineering construction. *E3S Web Conf.* **2019**, *97*, 05004. [CrossRef]
24. Sharma, S.; Sachan, P.B.; Kumar, N.; Ranjan, R.; Kumar, S.; Poddar, K. Vortex breakdown control using varying near axis swirl editors-pick. *Phys. Fluids* **2021**, *33*, 093606. [CrossRef]
25. Wang, Z.; Yu, B.; Chen, H.; Zhang, B.; Liu, H. Scaling vortex breakdown mechanism based on viscous effect in shock cylindrical bubble interaction. *Phys. Fluids* **2018**, *30*, 126103. [CrossRef]
26. Oberleithner, K.; Paschereit, C.; Seele, R.; Wygnanski, T. Formation of turbulent vortex breakdown: Intermittency, criticality, and global instability. *AIAA J.* **2012**, *50*, 1437–1452. [CrossRef]
27. Wang, Y.; Wang, X.; Yang, V. Evolution and transition mechanisms of internal swirling flows with tangential entry. *Phys. Fluids* **2018**, *30*, 013601. [CrossRef]
28. Rukes, L.; Sieber, M.; Paschereit, C.; Oberleithner, K. The impact of heating the breakdown bubble on the global mode of a swirling jet: Experiments and linear stability analysis. *Phys. Fluids* **2016**, *28*, 104102. [CrossRef]
29. Ortiz, S.; Donnadieu, C.; Chomaz, J.-M. Three-dimensional instabilities and optimal perturbations of a counter-rotating vortex pair in stratified flows. *Phys. Fluids* **2015**, *27*, 106603. [CrossRef]
30. Batchelor, G.K. *Introduction to Fluid Dynamics*; Cambridge University Press: Cambridge, UK, 2002.
31. Grabowski, W.J.; Berger, S.A. Solutions of the Navier–Stokes equations for vortex breakdown. *J. Fluid Mech.* **1976**, *75*, 525–544. [CrossRef]
32. Leibovich, S. The structure of vortex breakdown. *Ann. Rev. Fluid Mech.* **1978**, *10*, 221–246. [CrossRef]
33. Garg, A.K.; Leibovich, S. Spectral characteristics of vortex breakdown flowfields. *Phys. Fluids* **1979**, *22*, 2053–2064. [CrossRef]
34. Batchelor, G.K.; Gill, A.E. Analysis of stability of axisymmetric jets. *J. Fluid Mech.* **1962**, *14*, 529–551. [CrossRef]
35. Akhmetov, V.K. Numerical and asymptotic flow stability analysis of vortex structures. *E3S Web Conf.* **2021**, *263*, 03003. [CrossRef]
36. Akhmetov, V.K.; Shkadov, V.Y. Stability of a free vortex. *Moscow Univ. Mech. Bull.* **1987**, *42*, 17–22.
37. Akhmetov, V.K.; Shkadov, V.Y. New viscous mode of free vortex instability. *Fluid Dyn.* **1999**, *34*, 839–841.